16TH EUROPEAN CONFERENCE ON EARTHQUAKE ENGINEERING THESSALONIKI 18 - 21 JUNE 2018

CALIBRATION OF SEISMIC HAZARD MAP USING HISTORICAL EARTHQUAKES—A CASE STUDY IN SHANXI RIFT SYSTEM, CHINA

Danhua XIN[1], Friedemann WENZEL[2]

ABSTRACT

The Shanxi Rift System, situated at the east margin of the Ordos Block, is a seismically highly active area in North China. According to historical records, at least 7 MS ≥7.0 earthquakes have occurred in this region since the first earthquake was documented in 231 B.C. in Shanxi and caused serious casualties and damage. A relatively complete catalog of historical earthquakes with magnitude≥5 in Shan Rift System can be dating back to 1458B.C. In this study, our comprehensive hazard model is generated using open source software CRISIS based on available geological and geophysical information currently. The consistency of the hazard model with historical earthquake (both calculated with same ground motion attenuation model) is checked. The results are shown in the form of return periods.

Keywords: PSHA; Hazard Map; Return Period; Shanxi Rift System

1. INTRODUCTION

Seismic hazard maps predict the effects of future earthquakes of different magnitudes by assuming distributions of earthquakes within seismic source zones, and using ground motion attenuation relations to specify how shaking decreases with distance from the epicentre. The hazard in a given location is described by the exceedance probability of various ground motion levels caused by earthquakes that are expected to happen in a given period of time.

Since the significant role played by a national seismic hazard map in setting construction standards and, more generally, in prioritizing risk mitigation efforts (Sørensen et al., 2012), it is essential to calibrate the modelled hazard map using discrete historical earthquakes, considering the epistemic and aleatory uncertainties embedded in the modelling process.

The Shanxi Rift System, located in the west of the North China Plain and the east of the Ordos Block, is one of the most active seismic zones in China, with the characteristics of high earthquake intensity and occurrence frequency. To the south it's bounded by the Sichuan Basin, the Qinling Mountains and the Weihe Basin, with the Taihang Mountains located in the eastern margin of the Shanxi rift system. The northward extrusion of the Indian Plate not only leads to the vertical uplift of the Tibet Plateau, but also to obvious lateral movements (Wang et al., 2001). Eastward flow of the Tibet Plateau material is hindered by the Sichuan Basin. Thus the movement is further divided into a northeast lateral movement and a southeast lateral movement. The push during the northeast lateral movement of the Tibet Plateau together with the blocking function of the North China Plain lead to anti-clock rotation of the Ordos Block, which magnifies the seismicity in the Shanxi Rift System (Peltzer et al., 1996; Zhang et al., 1998; Li et al., 2005). Historically, the largest earthquakes in the Shanxi Rift were

[1]PhD Student, Karlsruhe Institute of Technology (KIT), Karlsruhe, Germany, danhua.xin@kit.edu
[2]Professor, Geophysics Institute, KIT, Karlsruhe, Germany, friedemann.wenzel@kit.edu

the Hongdong Mag 8 earthquake in 1303, the Huaxian Mag 8.3 earthquake in 1556 and the 1695 Linfen Mag 7.8 earthquake (Figure 1). The Huaxian event was the deadliest known earthquake in human history. Itcaused more than 800,000 fatalities.

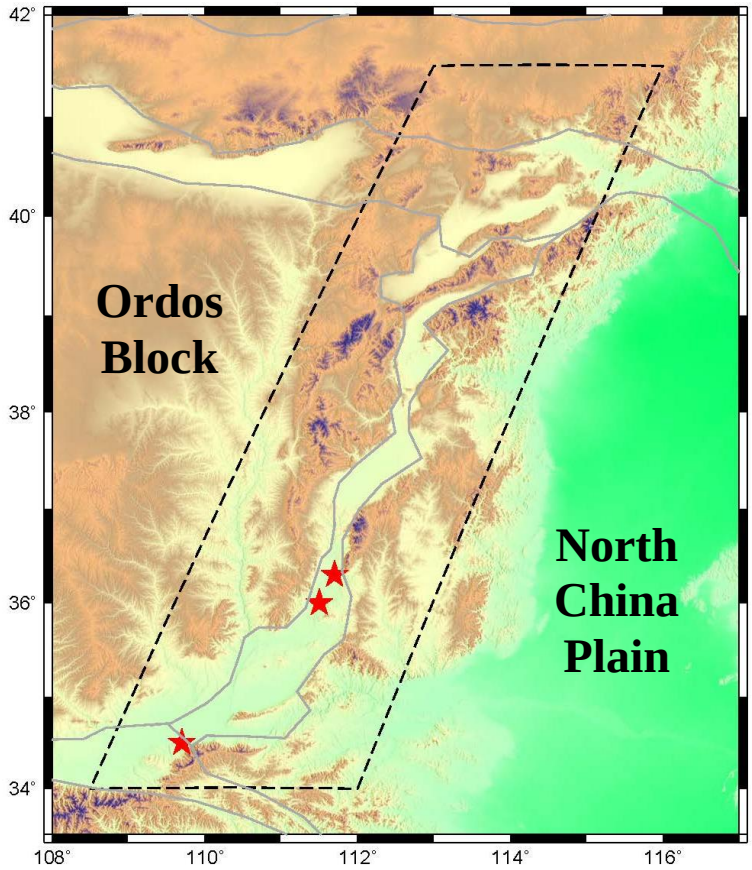

Figure 1: Tectonic background of the Shanxi Rift System

2. METHODS IN SEISMIC HAZARD MAP GENEARATION

The most common approach to generate a hazard map is to consider all the possible earthquakes that could cause significant shaking at a place. This method called probabilistic seismic hazard assessment or PSHA, involves estimating the probable shaking from all different magnitude earthquakes and producing an estimate of the combined hazard. It was developed by Cornell (1968) and is widely applied in engineering design (e.g. McGuire, 1995).

There are four steps to generate a hazard map. Firstly, the identification of seismic sources (both area sources and fault sources), which is mainly based on geological structure and previous seismicity in research area. Secondly, to characterize the distribution of earthquake magnitudes for each seismic source, namely the Gutenberg-Richter relationship. Thirdly, the development of ground motion attenuation relationship, which relates the earthquake ground motion at the site of interest to the magnitude, distance and local site conditions. Fourthly, combining information from previous steps to compute the annual rate of exceeding a given ground motion intensity, as shown in formula (1).

$$\lambda(IM > x) = \sum_{i=1}^{n_{sources}} \lambda(M_i > m_{\min}) \sum_{j=1}^{n_M} \sum_{k=1}^{n_R} P(IM > x \mid m_j, r_k) P(M_i = m_j) P(R_i = r_k) \quad (1)$$

In which $\lambda(IM > x)$ represents the annual rate of exceeding ground motion value x ;

$n_{sources}, n_M, n_R$ represents the number of seismic sources, magnitude bins and distance bins respectively; $\lambda(M_i > m_{\min})$ represents the annual occurrence rate of the minimum magnitude threshold; $P(IM > x \mid m_j, r_k)$ describes the probability of exceeding ground motion value x given a certain magnitude and distance. It is usually modelled as cumulative lognormal distribution. The inverse of the annual ground motion exceedance rate is the return period of the respective ground motion level.

Within a given PSHA model, ground-motion level and return period are interchangeable. The abscissa of a hazard curve at one site can be expressed in either the ground-motion level or the return period. Therefore, the same return period will represent different ground-motion levels at different sites (Mak and Schorlemmer, 2016). The return periods of hazard maps of interest are generally within the range of 100 to 2475 years are generated, corresponding to 2-40 percent probability of exceedance within 50-year of various ground motion levels.

The main objective of this study is to test the probabilistic seismic hazard model performance using historical records specifically for the Shanxi Rift System. Thus we established four PSHA hazard maps that use the source and ground motion attenuation models of a previous study (Bin Li, 2015) for the return periods 101, 475, 975, and 2475 years. In order to test the compatibility of those hazard maps with the historic catalogue we calculate hazard using the historical catalogue data instead of the source models, with the same ground motion attenuation model as used in Bin Li (2015) for ground motions that relate to the PSHA return periods. For instance, for T_{R1} =101 year we get from the PSHA hazard map for each site *i* the respective ground motion values z_{1i} and in the same way for *k=2, 3, 4* representing T_{R2}*=475*, T_{R3}*=975*, T_{R4}*=2475* year. The annual exceedance rate (hazard) of a ground motion level z_k, that has been established in the PSHA map at site *i*, caused by all *Nc* historical earthquakes during the catalogue time *Tc* can be expressed as follows:

$$\lambda_i(IM \geq z_{k,i}) = \frac{1}{T_C} \sum_{n=1}^{N_C} \left[1 - \Phi\left(\frac{z_{k,i} - g(m_n, r_{i,n})}{\sigma}\right) \right] \tag{2}$$

The corresponding "calibrated" return period using all historical earthquakes at site *i* for ground motion level z_k is:

$$\hat{T}_{Rk,i} = \frac{1}{\lambda_i(IM \geq z_{k,i})} \tag{3}$$

When taking all sites *Ns* into consideration, the mean "calibrated" return period for the research area is expressed as:

$$\hat{T}_{Rk} = \frac{1}{\frac{1}{N_S} \sum_{i=1}^{N_S} \lambda_i(IM \geq z_{k,i})} \tag{4}$$

In case of compatibility of the PSHA with the catalogue information we expect that approximately:

$$\hat{T}_{Rk} \approx T_{Rk} \tag{5}$$

3. DATA SOURCES

The seismic parameters we used to establish seismic hazard model in Shanxi Rift System is mainly based on the doctoral work of Bin Li (through personal communication), including the zonation of 28 area sources and 21 fault sources (Figure 2), with the assumption that Mag 6 earthquakes and above are related to fault sources and earthquakes below Mag 6 are assumed to occur in area sources.

For calibration of the hazard model, the historical earthquake catalogue is downloaded from *http://data.earthquake.cn* for both history earthquake records (1831B.C.~1969A.D.) and modern instrumental records since 1970 A.D. provided by China Earthquake Data Center.

Assuming that the ground motion generated by earthquakes below this limit is not disastrous, the minimum magnitude of earthquakes used both in the PSHA hazard model and in historical catalogue is Mag 5 (Figure 2). The ground motion attenuation relationship used is from Yu (2013), which is specially designed and occupied in the generation of China's Fifth National Seismic Zonation Map issued in 2016. The historical earthquake catalogue is declustered using the method in Reasenberg (1985) before put into further use.

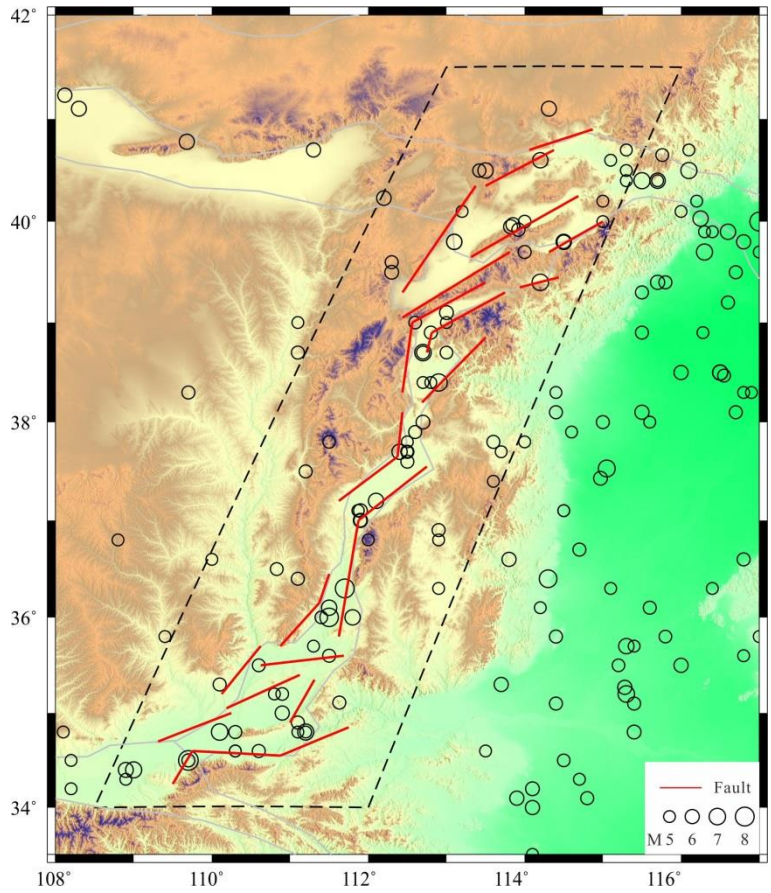

Figure 2: Distribution of fault sources and historical earthquakes with magnitude 5 and above.

4. RESULTS

Given the seismic parameters required in PSHA method to generate a seismic hazard map, we use the open source software "CRISIS2015", developed by Ordaz et al. (2013) for computing seismic hazard, to generate our hazard maps for interested return periods 101-yr, 475-yr, 975-yr and 2475-yr (Figure 3). The resolution of the grid point in each map is 0.05 °×0.05 °, approximately 5km×5km. With the increase of return periods, the corresponding PGA values are also magnified, which is straightforward to check from Figure 3. According to formula (2) ~ (4) in the methods part, the calibrated return period calculated using historical catalogue are also plotted for four return periods (Figure 4).

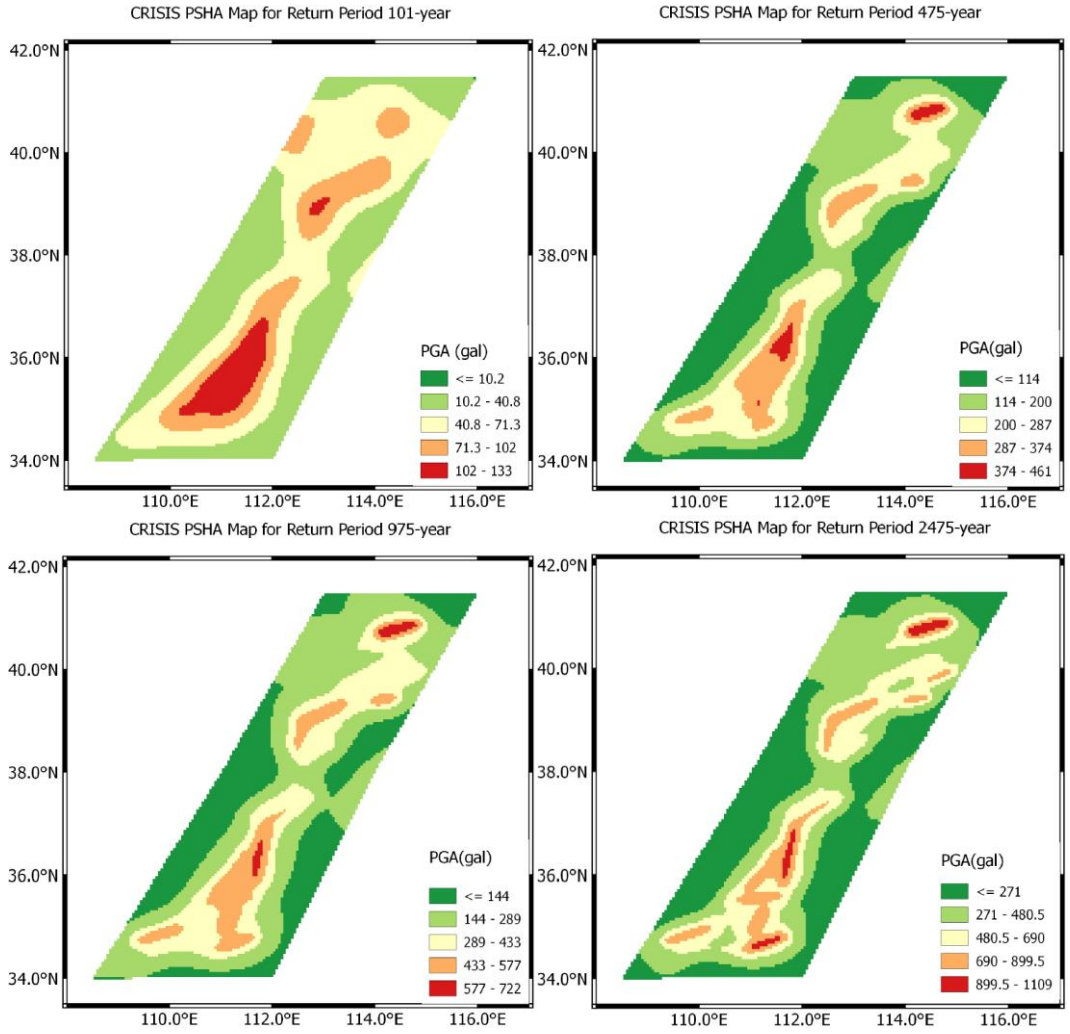

Figure 3: Modelled hazard maps using CRISIS2015 based on PSHA method for return period 101-yr, 475-yr, 975-yr and 2475-yr, respectively (unit: gal, 1g=981gal).

The four maps in Figure 4 represents that when k=1, 2, 3, 4, return period T_{Rk} = 101-year, 475-year, 975-year and 2475-year. The different colors represent the five ranges of calibrated return period at each grid. For example, when T_{Rk} = 101-year, the five ranges from green to red are "$\leq T_{Rk}/2$, $T_{Rk}/2 \sim T_{Rk}$, $T_{Rk} \sim 2T_{Rk}$, $2T_{Rk} \sim 5T_{Rk}$, $\geq 5\ T_{Rk}$.

If the modeled hazard in CRISIS2015 is in consistent with historical observation, we expect that the calibrated return period at each grid $\hat{T}_{Rk,i}$ is approximately equal to T_{Rk}, thus the color in each plot are expected more in lightgreen ($\hat{T}_{Rk,i} \in [T_{Rk}/2, T_{Rk}]$) or yellow ($\hat{T}_{Rk,i} \in [T_{Rk}, 2T_{Rk}]$). Statistically, the percentage of lightgreen/yellow girds is 62%, 61%, 45% and 25%, corresponding to the return period of 101-year, 475-year, 975-year, 2475-year.

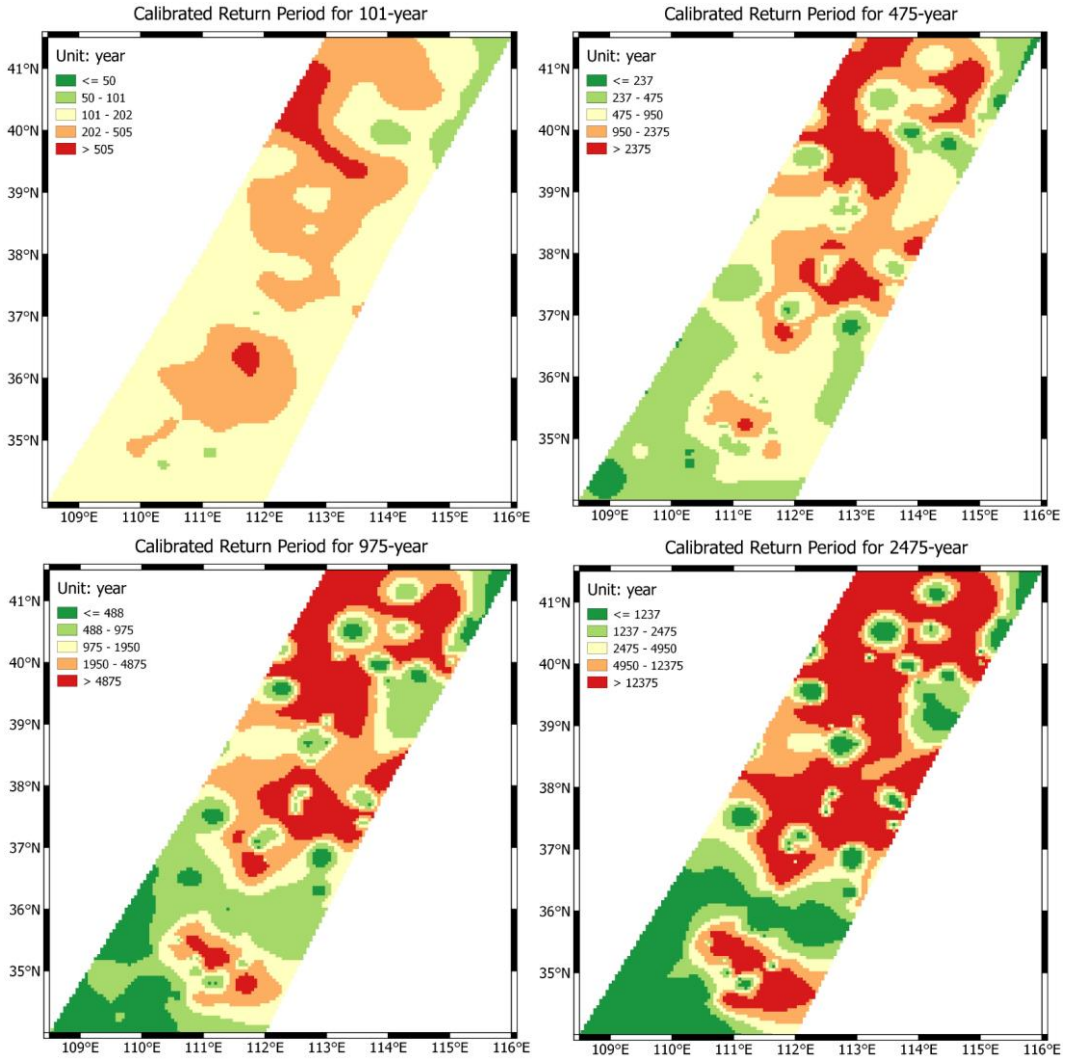

Figure 4: The calibrated return period calculated using historical earthquakes corresponding to return period 101-yr, 475-yr, 975-yr and 2475-yr. In each color bar, "five colors" (from green to red) represent that the calibrated return period at each grid point $\hat{T}_{Rk,i}$ is within the range of "$\leq T_{Rk}/2$, $T_{Rk}/2 \sim T_{Rk}$, $T_{Rk} \sim 2T_{Rk}$, $2T_{Rk} \sim 5T_{Rk}$, $\geq 5 T_{Rk}$" correspondingly.

5. DISCUSSION AND CONCLUSION

Suppose the PSHA model is correct and compatible with historical observations, since the historical catalogue length is around 550-year long, ideally if the return period is small (101-yr, 475-yr) compared to the catalogue time, we expect $\hat{T}_R \approx T_R$; if the return period is large (975-yr, 2475-yr), due to the "catalogue-length effect" that the limited observation time should lead to $\hat{T}_R > T_R$;

However, if there is discrepancy between the historical observation and model prediction, as our results have shown that for small return period $\hat{T}_R > T_R$, and for large return period $\hat{T}_R < T_R$ (see Table 1 below). This can be explained from the following two aspects, as indicated from Figure 5.

Table 1. Average calibrated return period for four return period 101-yr, 475-yr, 975-yr and 2475-yr.

T_{Rk}	$\hat{T}_{Rk}$
101	204
475	691
975	1149
2475	1959

Possible explanations for the discrepancy between the PSHA hazard model and historical observations can be explored from Figure 5:

- **a)** We have more high magnitude events (mag$\geqslant$7.5) in the catalogue as compared to the model. Since large magnitude events place a crucial role in determining ground motion when the return period is relatively large (975-yr, 2475-yr), in this case $\hat{T}_R < T_R$.
- **b)** We have less low magnitude (mag$\leqslant$6) events in the catalogue as compared to the model. Since low magnitude events place a crucial role in determining ground motion for short return period (101-yr, 475-yr), thus $\hat{T}_R > T_R$.

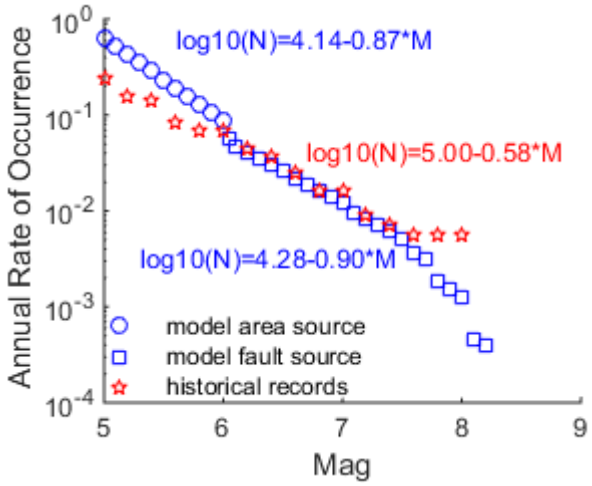

Figure 5: Annual occurrence rate of Mag 5 and above EQs in CRISIS source model and historical catalog.

To conclude, in our calibration of seismic hazard map generated using PSHA method in CRISIS using historical earthquake records, we find out that, for small return periods (101-yr, 475-yr) $\hat{T}_R > T_R$, and for large return periods (975-yr, 2475-yr) $\hat{T}_R < T_R$. This result reveals the discrepancy between modelled hazard and actual historical observation, which provides a basic idea of comparing hazard model prediction using discrete earthquake records.

6. ACKNOWLEDGMENTS

Sincere thanks will be given to Bin Li for providing the seismic parametric data in his PhD work. We're grateful to China Earthquake Data Centre for the historical and instrumental earthquake catalog. The CRISIS series software developed by Ordaz et al. has provided great help in this research, which is deeply appreciated.

7. REFERENCES

Cornell CA (1968). Engineering seismic risk analysis. *Bulletin of the seismological society of America*, *58*(5),

1583-1606.

Li B (2015). Seismotectonics and seismic hazard of the Shanxi Rift System, North China, *Ph.D. Thesis*, Faculty of Mathematics and Natural Sciences, UNIVERSITY OF BERGEN, Norway.

Li YX, Zhang JH & Guo LQ (2005). Couterclockwise rotation and geodynamics of Ordos Block [J]. *Crustal Deformation and Earthquake*, *3*, 010.

Mak S, & Schorlemmer D (2016). A comparison between the forecast by the United States National Seismic Hazard Maps with recent ground-motion records. *Bulletin of the Seismological Society of America*, *106*(4), 1817-1831.

McGuire RK (1995). Probabilistic seismic hazard analysis and design earthquakes: closing the loop. *Bulletin of the Seismological Society of America*, *85*(5), 1275-1284.

Ordaz M, Martinelli F, D'Amico V, & Meletti C (2013). CRISIS2008: A flexible tool to perform probabilistic seismic hazard assessment. *Seismological Research Letters*, *84*(3), 495-504.

Peltzer G & Saucier F (1996). Present-day kinematics of Asia derived from geologic fault rates. *Journal of Geophysical Research: Solid Earth*, *101*(B12), 27943-27956.

Reasenberg P (1985). Second-order moment of central California seismicity, 1969–1982. *Journal of Geophysical Research: Solid Earth*, *90*(B7), 5479-5495.

Sørensen MB, Spada M & Babeyko A, Wiemer S, Grünthal G (2012). Probabilistic tsunami hazard in the Mediterranean Sea. *Journal of Geophysical Research: Solid Earth*, *117*(B1).

Wang Q, Zhang PZ, Freymueller JT, Bilham R, Larson KM, Lai XA, ... & Liu J (2001). Present-day crustal deformation in China constrained by global positioning system measurements. *science*, *294*(5542), 574-577.

Yu YX, Li SY & Xiao L (2013). Development of Ground Motion Attenuation Relations for the New Seismic Hazard Map of China. *Technology for Earthquake Disaster Prevention*, *8*(1), 24-33, in Chinese

Zhang YQ, Mercier JL & Vergély P (1998). Extension in the graben systems around the Ordos (China), and its contribution to the extrusion tectonics of south China with respect to Gobi-Mongolia. *Tectonophysics*, *285*(1-2), 41-75.